THE ASTROPHYSICAL JOURNAL, 426:150–158, 1994 May 1

HUBBLE SPACE TELESCOPE OBSERVATIONS OF PLANETARY NEBULAE IN THE MAGELLANIC CLOUDS. II. SMP 85, A YOUNG PLANETARY

MICHAEL A. DOPITA,[1] EMANUEL VASSILIADIS,[2] STEPHEN J. MEATHERINGHAM,[1] HOLLAND C. FORD,[2] RALPH BOHLIN,[2] PETER R. WOOD,[1] THEODORE P. STECHER,[3] STEPHEN P. MARAN,[3] AND J. PATRICK HARRINGTON[4]

Received 1993 October 25; accepted 1993 November 4

ABSTRACT

We have obtained *Hubble Space Telescope* Planetary Camera images in the [O III] λ5007 Å emission line, and FOS UV spectrophotometry of the low-excitation planetary nebula SMP 85 in the Large Magellanic Cloud. By combining these results with existing optical spectrophotometry, absolute flux measurements, and dynamical and density information, we have been able to construct a fully self-consistent nebular model. This proves that SMP 85 is a dense, young, carbon-rich object which started to be ionized about 500–1000 years ago, and which contains a substantial inner reservoir of atomic or molecular gas, probably in the form of many small cloudlets. These cloudlets have been ejected at a velocity not exceeding 6 km s^{-1}, a result which, together with the morphology is an important clue to mass loss during late AGB evolution. We have directly detected the central star through its UV continuum emission, and from both Zanstra techniques and nebular modeling derive a stellar temperature of 46000 ± 2000 K, a stellar luminosity of 7300 ± 700 $L_\odot$, and a core mass of 0.63–0.67 $M_\odot$. The nebular analysis also demonstrates that there is severe depletion of the nebular gases onto dust grains, most likely of the calcium magnesium silicate variety; a surprising result in view of the carbon-rich nature of the ionized nebula.

Subject headings: Magellanic Clouds — planetary nebulae: individual (SMP 85)

1. INTRODUCTION

The evolution of stars from the termination of the asymptotic giant branch (AGB) evolution through the planetary nebula (PN) stage represents an important transition, the parameters of which are still poorly determined from an observational viewpoint. The major reason for this is the absence of a reliable distance scale for Galactic PNs, which has proved to be a millstone around the neck of progress. However, the distance problem can be overcome by the study of the population of PNs in the Galactic bulge, or in the Magellanic Clouds. Of these, the Magellanic Cloud group is a vital key to understanding the details of post-asymptotic giant branch evolution. The distance is well known, and unlike the Galactic bulge group, reddening is generally small. Furthermore, these PNs are near enough to be easily studied, and details of their internal structure can be resolved with the *Hubble Space Telescope* (*HST*).

In the optical, the Magellanic Cloud population has been the subject of a systematic and detailed study by us and by the University College group in recent years, and data on the diameters, fluxes, expansion velocities, and kinematics have been accumulated (see the review by Barlow 1989; also Dopita et al. 1985b; Dopita, Ford, & Webster 1985a; Meatheringham et al. 1988a; Meatheringham, Dopita, & Morgan 1988b; Wood, Bessel, & Dopita 1986; Wood et al. 1987; Jacoby, Walker, & Ciardullo 1990).

However, the key to the determination of the PN nebular abundances, and the position of the central star on the H-R diagram is accurate spectrophotometry over as wide a wavelength range as possible. With the aid of a photoionization code, the ionization temperature can be determined from the nebular excitation, the luminosity of the central star can be determined from the absolute Hβ flux, and the chemical abundances can be determined from the electron temperature of the nebula and from its detailed emission line spectrum. In a recent series of papers (Clegg et al. 1987; Meatheringham & Dopita 1991a, b; Vassiliadis et al. 1992), high-quality optical spectrophotometry has been obtained which has permitted such an investigation to be undertaken (Dopita & Meatheringham 1991a, b). However, this exercise remains incomplete without the high-resolution direct imaging and spectrophotometry that is possible using the *HST*. In particular, *HST* imaging will tell us the geometry of the nebular gas with respect to the planetary nebula nucleus (PNN), enable us to derive a dynamical age, and reveal whether the nebula is optically thin to the ionizing radiation. UV spectrophotometry with the Faint Object Spectrograph (FOS) will reveal the chemical abundance of key elements such as C, synthesized in helium-burning layers of the precursor star, dredged up into the hydrogen-rich envelope, and ejected into the nebular gas. Heavier atomic species such as Ca, Mg, and Si are best observed in the UV, and a study of the far-UV continuum gives us our best chance of discriminating the continuum produced by the PNN itself from the nebular continuum emission processes, especially when the star has a high effective temperature.

In the previous paper in this series (Dopita et al. 1993, hereafter Paper I), we described imaging observations of the extreme PN in the LMC, WS 35 in the catalog of Westerlund & Smith (1964), or SMP 83 in the catalog of Sanduleak, MacConnell, & Philip (1978). This was selected by the GTO team for observation with the Planetary Camera (PC) on the basis of its extreme velocity of expansion and other characteristics. We were able to combine the results of this imaging with the

[1] Mount Stromlo and Siding Springs Observatories, Institute of Advanced Studies, The Australian National University, Private Bag, Weston Creek P.O., ACT 2611, Australia.
[2] Space Telescope Science Institute, 3700 San Martin Drive, Homewood Campus, Baltimore, MD 21218.
[3] NASA Goddard Space Flight Center, Code 680, Greenbelt, MD 20771.
[4] Department of Astronomy, University of Maryland, College Park, MD 20742–2421.

published optical and UV spectrophotometry to generate a self-consistent photoionization model. This allowed us to place SMP 83 on the Hertzsprung-Russell diagram with reasonable accuracy and to prove that it was a PN derived from a high-mass precursor.

In this Paper, we give the first results of our Cycle I GO program comprising both imaging and spectrophotometry of a young, high-density PN, SMP 85 in the LMC. The long-term aim of this program is to make a systematic study of over 20 objects covering the full range of the Hertzsprung-Russell diagram accessible to observation with *HST*. By this means, we hope to ultimately place severe observational constraints on theoretical models, so as to cast light on the physical processses involved in AGB evolution and beyond.

2. RESULTS OF *HST* IMAGING

2.1. *Observations and Data Processing*

The LMC PN SMP 85 was observed with the PC on 1991 October 24 as part of our Cycle I GO program. To reduce the noise due to cosmic-ray events, two sequential exposures of 600 s were made in the [O III] λ5007 line using the F502N filter. This gave a peak signal to noise in excess of 20 per pixel. The wavelength of peak transmission of the [O III] filter is 5016 Å, and its bandpass is 30 Å, FWHM. The PN was placed on the PC8 chip in order to provide maximum sensitivity, and displaced $\sim$15″ northeast from the center of the chip in order to avoid the Baum Spot. At the time of observation, PSF observations for this chip and this filter were not available. To enable us to correct the data for the effects of the spherical abberation of *HST*, we preceded the *HST* observations of the PN by three sequential exposures of 800 s of a $V = 13.05$ star some 26″ from the PN, the star having been placed on the same point of the PC8 chip as the PN. Of the three exposures, only the first two could be used in the construction of the PSF, since the third was affected by a reaquisition problem. The two remaining exposures gave us a measured PSF with a peak S/N of greater than 30 per pixel, which could then be used in the subsequent image processing.

The STSDAS task CALWFPC was used to reprocess the images, using the bias subtraction and flat field correction available on 1992 May 5. Since calibration of the [O III] filter was relatively low on the list of calibration priorities, the gap between the time of the observations and the time when the calibration was obtained was inevitable. However, we have no reason to believe that this has any deleterious effect on the quality of the reductions. In order to deconvolve the data, a 256 × 256 pixel sub-image centered on the PN was extracted and cleaned of cosmic ray hits. A standard Lucy (1974) deconvolution was done using 70 interactions. Since the point spread function (PSF) was explicitly determined by calibration observations with this filter, it was not necessary to use the pre-launch *HST* optical model in the code TINYTIM (Krist 1992). In any case this model seems to be inadequate, since fainter features in the observed PSF were not reproduced by the corresponding TINYTIM model. We found that application of more than 100 iterations tended to amplify both noise features and artifacts in the image (see Paper III, in preparation).

2.2. *The Size and Dynamical Age of SMP 85*

We show in Figure 1*a* the original PSF as measured above for the F502N filter and in Figure 1*b* this same PSF deconvolved using the Lucy algorithm. Each frame is 5.″5 square. This clearly demonstrates the power of the deconvolution technique. In Figure 2, we show that central 1.″0 × 1.″0 of the PN frame and of the PSF, after deconvolution. To do justice to the large dynamic range of the observations, these are shown at three gray levels, separated from each other by 0.5 dex in intensity. It is clear that the PN is well resolved at all levels, is almost perfectly round, and has very little internal structure other than that which would be produced by a radial density gradient. Its structure is similar to low-excitation Galactic PNs such as IC 418, IC 3568, or BD +30°3639 (see Balick 1989). In order to determine the radial brightness gradient we used the

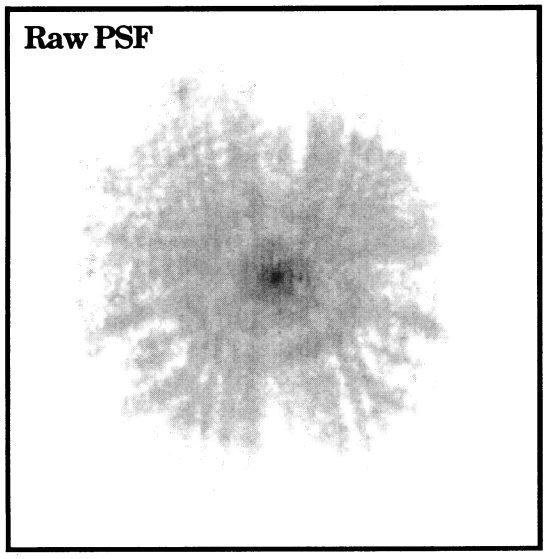

FIG. 1*a*

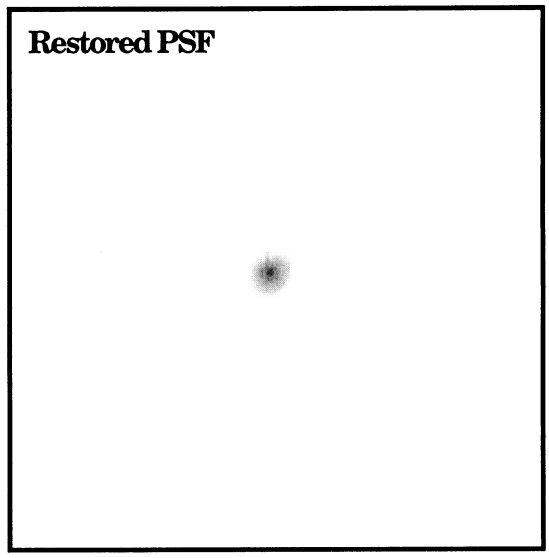

FIG. 1*b*

FIG. 1.—(*a*) Raw PSF on the PC8 chip measured through the F502N filter. The gray scale here is logarithmic so as to bring out the fainter features in the PSF. (*b*) PSF after 70 iterations with the Lucy (1974) algorithm. Note that 94% of the light now follows on the central 0.″043 pixel, and that the first diffraction maximum of the intrinsic telescope PSF can now be distinguished.

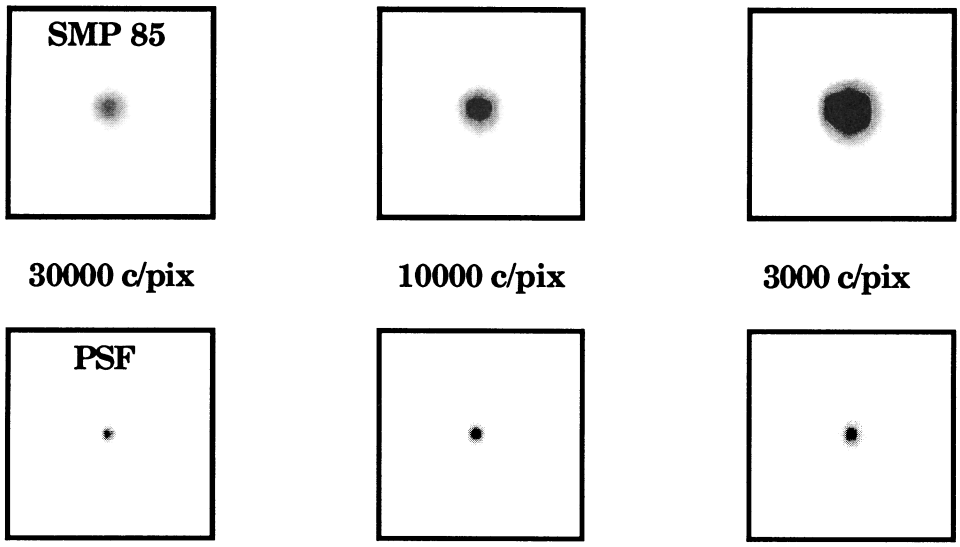

FIG. 2.—Deconvolved image of the PN (*top*) and of the PSF (*bottom*) are shown on a linear scale at three different intensity levels to demonstrate the very high dynamic range achieve. The size of the frame is 1″.0. Note that the PN is very clearly resolved, but that it does not have a pronounced outer boundary.

Galaxy Aperture Surface Photometry (GASP) software. The results of this is shown in Figure 3. It is clear that the PN has a bright core with a radius of ~3.5 pixels (~0″.1) which corresponds to $\sim 7.5 \times 10^{16}$ cm at the distance of 49 kpc we have assumed as being the distance of the LMC (Feast & Walker 1987; Feast 1988). Outside this core, the profile falls off with angular radius θ approximately as θ^{-3} as far as the outer boundary at 0″.34 ($\sim 2.4 \times 10^{17}$ cm). For a large nebula, this radial variation translates to a local emission profile having r^{-4}, which, at constant [O III] emissivity could be produced by a density gradient following a density law r^{-2}.

Dopita et al. (1988) measured the expansion velocity of SMP 85 to be 11.3 km s^{-1} in the [O III] λ5007 line and 11.2 km s^{-1} in the [O II] λ3727 line. This is very similar to the sound speed in the ionized material; 12.4 km s^{-1}, suggesting that the ionized gas in flowing out under its own thermal energy, rather than being accelerated by a strong stellar wind. Taking the dynamic age to be the time taken for the gas to flow out of the dense core of the nebula, we can estimate a (maximum) dynamical age of ~2000 years.

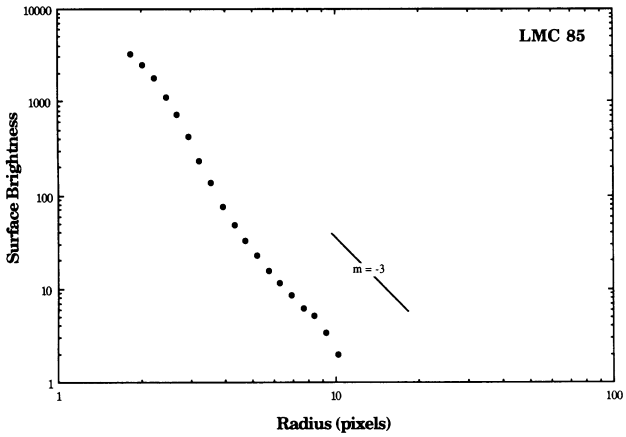

FIG. 3.—Radial intensity profile of SMP 85 measured using the GASP routine. For comparison a radial power-law gradient following an r^{-3} law is also shown.

3. RESULTS OF *HST* SPECTROSCOPY

3.1. *Observations and Data Processing*

The FOS observations were carried out in a single orbit on 1993 January 6. Because the PN was very small, it was acquired by a binary acquisition, followed by an IMAGE exposure. From this, the PN was confirmed to have been centered in the 1″.0 circular aperture to a precision of ~0″.12. The science exposures consisted of sequential exposures using the blue side of the detector in each of the G130H, G190H, G270H, and PRISM dispersive elements. The three grating give continuous coverage in wavelength from 1150–3250 Å. Since the grating observations suffer flux calibration uncertainty through spherical abberation losses, uncertainty in the sensitivity calibration and errors due to decentering the magnetically induced drifts of the electron image on the Digicon detector diode array, we took the prism observations so as to provide overlap with the ground-based spectrophotometric data.

The data were processed through the STSDS software to provide flat-field, sensitivity and scattered light corrections. The latter correction was necessary only for the G130H observation, where scattered light proved to be only 0.002 counts s^{-1}.

The optical spectrophotometry of Meatheringham & Dopita (1991a) was normalized so as to give an Hβ flux of 3.802×10^{-13} ergs cm^{-2} s^{-1} corrected to above the Earth's atmosphere, as measured by narrow-band filter photometry by Meatheringham, Dopita, & Morgan (1988b). The prism observations, after deblending from the [O III] lines indicated a somewhat lower Hβ flux of 2.6×10^{-13} ergs cm^{-2} s^{-1}. For the Hγ + [O III] line blend the agreement is poorer still; 1.74×10^{-13} ergs cm^{-2} s^{-1}, from the optical spectrophotometry, compared with the 0.77×10^{-13} ergs cm^{-2} s^{-1} obtained from the prism data. If the calibration for the prisim is correct, then it is clear that the abberation losses and losses due to

decentering have conspired to cause the prism to give an underestimate of the true flux. In order to correctly normalize the UV data to the optical, we normalize the UV data so that it gave the same integrated flux as the optical data in the range 3500–4700 Å.

The raw data clearly showed the 2200 Å interstellar absorption feature. In order to correct the UV data for the absorption of interstellar dust, we applied a combined LMC + Galactic extinction correction using the fitting parameters given by Fitzpatrick (1985) for the LMC, and by Seaton (1979) for the Galaxy. In the optical, we used the Whitford reddening function as tabulated by Kaler (1976). The mean logarithmic reddening constant, $c = 0.255$ derived from the Balmer decrement (Meatheringham & Dopita 1991a, b) was assumed, and 28% of this was assumed to be due to Galactic dust [$E(B-V) = 0.05$; Bessell 1991].

3.2. *Results*

The combined, extinction corrected spectra are shown in Figure 4 on an absolute flux scale. The Balmer Discontinuity appears in emission, and the spectrum rises strongly at the shortest wavelengths as a result of the contribution of the continuum of the underlying PNN. A number of prominent emission lines are visible in the UV spectrum. These include the Lyα line, which is a blend of both nebular and geocoronal components, the C III] $\lambda\lambda$1907, 1909 and C II] $\lambda\lambda$2325, 2329 doublets, and the [O II] λ2470 line. In addition, a number of absorption lines can be seen. Some of these can definitely be ascribed to interstellar absorption. These include the Mg II λ2800 line and the Fe II doublet near 2580 Å. However, the origin of the C IV $\lambda\lambda$1548, 1550 and the N V $\lambda\lambda$1239, 1243 absorption features is more problematic. Some of this absorption may be stellar in origin. However, to pre-empt the results of the following section, the relative strengths of the nebular and stellar continuum fluxes show that the depth of the absorption is greater than that which could be accounted by stellar atmospheric absorption alone. Clearly then, at least some of the absorption is also interstellar in origin. This conclusion is weakly supported by the absence of a Si IV stellar absorption feature, although the carbon-rich nature of the central star might well explain this.

Following the normalization with respect to the optical spectra described above, and also following the corrections for reddening the UV emission line fluxes relative to Hβ were extracted from the spectrum. These are listed in the third column of Table 1 along with the optical line intensities relative to Hβ measured by Meatheringham & Dopita (1991a, b). It is clear from the ratio of the [O II] λ2470 and the C II] $\lambda\lambda$2325, 2329 lines that the nebular gas has a high C/O ratio, expected if the PNN has evolved from a carbon star. These line

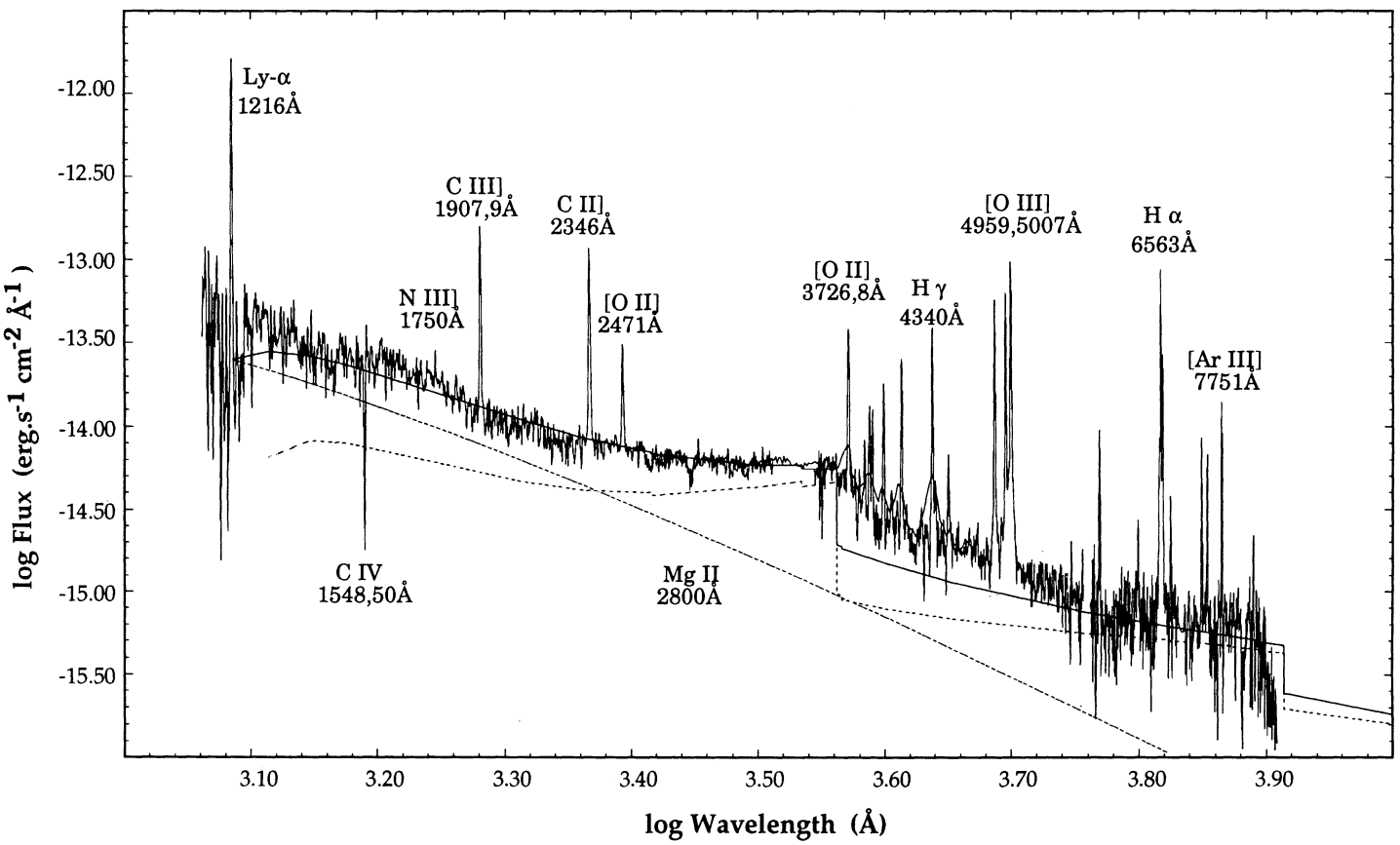

FIG. 4.—Merged *HST* and ground-based spectra corrected for interstellar extinction and plotted on an absolute flux scale by normalization to the observed Hβ flux. The dashed curve represents the theoretical nebular continuum for the model described in the text, and the dash-dotted line is a blackbody curve corresponding to 45,000 K, normalized so as to give the best fit to the observations at 1400 Å. The smooth solid curve is the sum of these, which gives a satisfactory fit to the observed continuum spectrum.

TABLE 1

OBSERVED AND MODELED LINE INTENSITIES WITH RESPECT TO Hβ = 100.0, ARRANGED BY WAVELENGTH

Ion	Wavelength (Å)	Observed	M69	M71	M91	M92	Best-Fit
N III]	1750	1.80	0.81	0.83	2.19	0.95	1.82
C III]	1907, 9	100.60	65.20	65.20	116.90	114.80	116.27
C II]	2326	102.60	49.80	35.85	37.88	279.60	110.40
[O II]	2471	20.80	11.60	7.50	6.42	47.97	18.89
C II, O III	2837	2.90					
He I	3188	2.00					
[O II]	3727, 9	35.80	19.60	44.40	71.22	3.76	50.98
Ne III]	3869	12.60	11.84	13.03	17.47	4.02	13.44
[S II]	4069, 76	2.70	3.31	2.05	0.30	10.15	3.26
Hδ	4100	23.10	25.95	25.90	25.93	26.25	26.03
Hγ	4340	46.20	46.87	46.82	46.87	47.13	46.95
[O III]	4363	3.20	1.85	1.98	3.12	2.65	2.98
He I	4472	5.70	4.72	4.64	4.67	4.37	4.58
Hβ	4861	100.00	100.00	100.00	100.00	100.00	100.00
[O III]	4959	117.30	90.38	94.94	154.10	13.67	111.97
[O III]	5007	338.00	260.30	273.50	443.90	39.40	322.55
[N II]	5755	1.30	1.10	0.69	0.81	8.52	3.12
He I	5876	12.00	13.08	12.91	12.90	11.87	12.59
[S III]	6312	1.20	3.26	2.42	0.47	1.80	0.87
[N II]	6548	15.10	9.77	12.95	15.98	4.16	12.43
Hα	6563	281.30	284.70	285.60	284.80	280.00	283.36
[N II]	6584	43.10	28.77	38.12	47.10	12.26	36.65
He I	6678	4.50	3.71	3.67	3.67	3.35	3.58
[Ar III]	7138	8.10	6.88	5.68	8.10	8.89	8.34
[O II]	7318, 28	30.30	15.52	10.04	8.55	63.50	25.03
[Ar III]	7751	2.50	1.66	1.37	1.95	2.14	2.01

fluxes will now be used to derive a photoionization model for the nebula to determine both physical conditions and nebular abundances.

4. PHOTOIONIZATION MODELING

4.1. *Single-Component Models*

According to the definition given by Dopita & Meatheringham (1991a, b) SMP 85 has an excitation class of 1.5. In the spectrum of Table 1, the strength of the [O II] λλ7318, 7328 with respect to the λλ3727, 3729 lines and the positive detection of the [S II] λλ4068, 4076 doublet without the λλ6717, 6731 lines are both indicators that this PN is unusually dense. This is in agreement with the high-resolution observations of the [O II] doublet by Dopita et al. (1988), which indicated a λλ3737/3729 line ratio near the high-density limit ($n_e > 50{,}000$ cm^{-3}).

Attempts were made by Dopita & Meatheringham (1991a, b) to model this and other PNs using the modeling code MAPPINGS 1 (Binette, Dopita, & Tuohy 1985). These assumed spherically symmetric, isobaric nebulae excited by a central star having a blackbody spectral distribution. In the case of SMP 85, a good fit to the optical spectrum could be obtained with an optically thick model, in which all the ionizing UV is absorbed by the surrounding nebular plasma. A C/O of 1.5 was assumed. For comparison with the results given in this paper, the specific parameters of the two photoionization models of Dopita & Meatheringham (1991a, b) are as follows, where the first and second numbers given refer to the first and second reference, respectively: Central star luminosity $L/L_\odot = 6150$; 7000, excitation temperature $T_{\rm eff} = 43{,}000$ K; 41,500 K, nebular density $N(\rm H) = 23{,}000$ cm^{-3}; 46,000 cm^{-3} (10,000 K, isobaric model), inner nebular radius $r_{\rm in} = 5 \times 10^{16}$ cm; 5×10^{16} cm, outer nebular radius, $r_{\rm out} = 8.8 \times 10^{16}$; 5.8×10^{16} cm, and nebular mass $M_{\rm neb} = 0.066$; $0.034\ M_\odot$. Clearly these two independent models are in quite good agreement with each other, most of the remaining differences being ascribable mainly to the different densities used in the modeling.

The UV data provide a number of valuable new observational constraints on the abundances of species that remain unobserved in the optical. In particular, as mentioned in the previous section, it is clear from the relative strengths of the [O II] λ2470 and the C II] λλ2325, 2329 lines that the nebular gas has a C/O ratio in excess of 2. Also, the nondetection of the Mg II resonance line at λ2800 [$I(2800) < 2.0$ with respect to $H\beta = 100$] places a strong constraint on the Mg abundance in the gaseous phase. To anticipate the results of our final model, the Mg abundance must be less than 2×10^{-7} by number with respect to hydrogen, consistent with a depletion onto grains of at least 150, by comparison with the LMC Mg abundance determination of 3×10^{-5} by Russell & Dopita (1992). The absence of the Si III λ2336 and Si III] λ1892 lines places a constraint on the Si abundance, $Z(\rm Si) < 6 \times 10^{-7}$ by number with respect to hydrogen, compared with the estimated LMC abundance of $\sim 2 \times 10^{-5}$; a depletion factor of order at least 30. Clearly then the gas-phase abundances are consistent with a severe depletion onto magnesium silicate dust grains. This is something of an extraordinary result, considering the carbon-rich nature of the number gas derived below, and begs the question, why is not the carbon locked up in grains (SiC, graphite, etc.) as well?

For the photoionization modeling presented here we have used the improved photoionization/shock modeling code MAPPINGS 2 (Sutherland & Dopita 1993). Amongst the improvements relevant to this exercise, this code now includes all important ionization stages up to fully stripped Fe and Ni, has a much improved adaptive spatial gridding procedure, explicitly computes all nebular continua, and operates with a much extended and improved set of atomic parameters, particularly with respect to the resonance and intercombination lines.

As a first test, we ran a model similar to those used in the original modeling exercise (spherically symmetric, optically thick, isobaric nebula excited by a central star having a blackbody spectral distribution). The effective ionization stellar temperature T_{ion} is constrained fundamentally by the ionization state of helium, and by the excitation of the other elements for which more than one species is observed. We can also derive constraints on T_{ion} through the electron temperature, and through the sum of all the strong emission lines with respect to Hβ, since this is the basis of the energy balance technique (Preite-Martinez & Pottasch 1984; Stoy 1933). The luminosity of the star is determined by matching the model Hβ luminosity to that which is observed, since this is a direct measure of the total number of ionizing photons. The density is determined by the density-sensitive ratios such as [O II] $\lambda\lambda$(7318, 7328)/(3727, 3279) [S II] $\lambda\lambda$ 4068, 4076/6717, 6731 and [O II] $\lambda\lambda$3737/3729.

The results of this simple model (model M69) are shown in Table 1. This model has stellar parameters which are quite similar to those given by the MAPPINGS I models, vis central star luminosity; $L/L_{\odot} = 7850$, excitation temperature $T_{eff} = 41{,}200$ K. However, in order to generate strong infrared [O II] lines along with strong UV [O II] and C II] lines, it was necessary to use a higher nebular density $N(H) = 61{,}000$ cm^{-3} (given for a temperature 10,000 K, in an isobaric model). To compensate for the lower ionization parameter, the inner radius had to be taken as small as $r_{in} = 4.4 \times 10^{14}$ cm, which led in turn to a small outer nebular radius, $r_{out} = 4.2 \times 10^{16}$; scarcely in agreement with the imaging. Other problems are apparent from the line fluxes in Table 1. First, the [O III] lines are weaker than observed, which, from the relationship between excitation class and effective temperature (Dopita & Meatheringham 1991b) would indicate that the effective temperature is too low. On the other hand the excitation defined from the [O III]/[O II] line ratios or the C III]/C II] ratio is apparently too high, which would indicate rather too high a temperature. A lowering of the effective temperature weakens all the forbidden and intercombination lines, in line with the energy balance arguments (Preite-Martinez & Pottash 1984), which makes the fit even worse. This cannot be compensated by an increase in elemental abundance, since the nebular temperature, which is already too low, would be further decreased, giving even weaker UV lines.

In order to have a fully self-consistent model, we should also strive to reproduce the image structure. As pointed out above, this should have a very steep radial density gradient. Photoionization models which have a density gradient as steep as r^{-2} do not have a stable solution, since the ionized nebula is either confined to a thin layer at the inner edge, with a thickness much smaller than the distance over which the characteristic density changes, or else the ionized nebula fills the whole region containing matter, and is optically thin. This is because in this case, the strength of the ionizing radiation decreases in the same way as the matter density, so as to keep a constant ionization parameter. Since our nebula is clearly optically, thick, based on the relative strength of the low-ionization species, this type of model does not apply. We have therefore taken a compromise density law, that in which density varies as $r^{-3/2}$. The "best-fit" model is also presented in Table 1; Model M71. This has precisely the same stellar parameters as M69. The nebula is characterized by a hydrogen density of 1.22×10^5 cm at a radius of 1.0×10^6 cm, and the ionized region extends out to 8.23×10^{16} cm; in somewhat better agreement with observation. This model fails mainly in that the low-excitation species occur in a region which has too low a density compared with observation. This is very well shown by the various [O II] lines; the λ2471 and the $\lambda\lambda$7318, 7328 lines are too weak, while the $\lambda\lambda$3737, 3739 lines are somewhat too strong.

4.2. *A Two-Component Model*

It is clear that we require a model having a strong density gradient to produce the image structure, having a higher stellar effective temperature to produce the required total forbidden line strength, but containing a very dense, optically thick zone of low-ionization parameter to reproduce the low-excitation species. Clearly this cannot be accomplished by a single component model.

We are therefore led to a model in which we have a reservoir of unionized dense gas near to the central star, either in the form of a set of cloudlets, or in the form of a coherent structure. This dense gas is rimmed by ionization fronts which produce mainly the low-excitation spectral lines, and gas flows from these ionization fronts stream into the intercloud region producing a more extended high-excitation emission region with a strong radial density gradient. Consistent with the constraints placed upon the procedure from the imaging and from the density-sensitive line ratios, we then seek linear sums of models for each of these components which produce as nearly as possible a constant ratio of observed to predicted line intensities over the full range of ionization states of a given element. If the abundance of an individual element is incorrect, then this will appear as an (approximately constant) offset in the ratio of observed to predicted line intensity over the whole range of ionization stages. The abundance can then be altered in a subsequent run so as to bring these ratios for that element to close to unity.

Within the constraints and assumptions of the two-component model itself, this procedure produces a fully self-consistent result, in that it agrees with the observed density and the physical size of the nebula, and also gives the correct global line strengths and excitation state of the nebula.

The parameters of our final model are given in Table 2, and the line intensities of this model are compared with the observations in Table 1. Here model M91 is for the intercloud component, and M92 refers to the contribution from the regions around the cloudlets. The intercloud medium is assumed to have a density profile varying as $r^{-1.5}$, which is nearly the steepest density profile for which a stable optically thick solution can be found. The [O III] emissivity profile for this solution follows a slope of close to $r^{3.3}$, and the outer radius of the [O III] zone is a 1.25×10^{17} cm, or 0".18 at the distance of the LMC. These figures are reasonably consistent with the imaging. The dense component probably occurs over a range of radii, but for the purposes of the modeling, we have placed it at the density-weighted mean radius of the intercloud component.

The "best-fit" model is obtained by adding the two components with relative weighting factors 0.7 and 0.3, respectively. The error on these numbers is about ± 0.1. Since both components are optically thick, these weighting factors are equivalent to the fractional covering factors for each component.

The comparison of the "best-fit" model with the observations is very good indeed. In Figure 5 we plot the observed and the theoretical line intensities for each element over all observed ionization stages. From this figure and Table 1, we

TABLE 2

INFERRED PARAMETERS FOR SMP 85 AND ITS NEBULA

A. INFERRED STELLAR PARAMETERS

Parameter	Value
$L/L_\odot$	7200 ± 600 (from nebular analysis) 7400 ± 1200 (from stellar continuum flux)
$T_{\rm eff}$ (K)	45000 ± 2000
$T_{\rm Zan}$ (K)	47800 ± 1900
$M/M_\odot$	0.63 ± 0.03 (if H-burning) 0.67 ± 0.03 (if He-burning)

B. ABUNDANCES OF THE ELEMENTS, BY NUMBER WITH RESPECT TO H (ERROR ~15%)

He	C	N	O	Ne	S	Ar
0.105	5.50E−4	4.27E−5	2.51E−4	3.02E−5	2.00E−6	1.74E−6

C. PROPERTIES OF NEBULAR COMPONENTS

Parameter	Value
Cloud Component, Model M91	
N(H) (cm^{-3})	1.6E6 (at 10,000 K, isobaric)
$\langle r \rangle$ (cm)	4.0E16
Covering factor	0.30 ± 0.08
$N_{\rm neb}$ ($M_\odot$)	4.13(±1.4)E−4
Intercloud Medium, Model M92	
N(H) (cm^{-3})	30600 (at r = 4.0E16 cm; N(H) ∝ $r^{3/2}$)
$r_{\rm in}$ (cm)	2.0E16
$r_{\rm out}$ (cm)	1.46E17
Covering factor	0.70 ± 0.08
$M_{\rm neb}$ ($M_\odot$)	0.075 ± 0.015

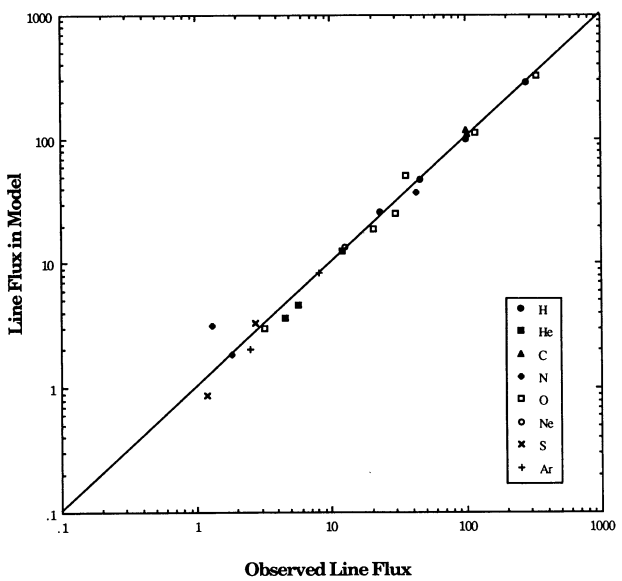

FIG. 5.—Line flux predicted for emission lines of each element in the models is plotted against the observed line flux with respect to Hβ = 1.0 for all unblended lines, and lines which represent the brighter component of a doublet with known intensities ratio. It is clear that the accuracy of the fit approaches that of the observations, and that the elemental abundances have been determined to an accuracy of order 15%.

see that the C II] line is produced mainly in the dense cloudlets, and the [O II] lines at λ2471 and λλ7318, 7324 are also strong in this phase. This removes the problems associated with the ionization state and apparent density of the single component models. As a consequence a higher effective temperature was indicated by the modeling, allowing generally stronger forbidden and intercombination lines relative to the recombination lines, and higher electron temperature.

The scatter of the points in Figure 5 is sufficiently small to give confidence that the elemental abundances have now been determined to within ±15%, which is comparable to the errors of the observations. The abundances found here can be compared with those obtained by Dopita & Meatheringham (1991a, b). The added constraints of the UV spectroscopy and the imaging allow us to have much more confidence in the abundance results. Overall, the heavy element abundances found in this study are higher than in the earlier work. This is a consequence of the increased number of cooling processes in MAPPINGS II, the inclusion of denser gas in the current model, and of the higher carbon abundance given by the UV data. The helium abundance found here is somewhat lower, thanks to the higher ionization temperature.

A final test of the comparison between theory and observation comes from consideration of the nebular continuum. In Figure 4 we plot the theoretical nebular and stellar continuua for the parameters determined by these models. The nebular processes included are the free-free, bound-free, and two-photon processes of both hydrogen and helium, allowing for collisional de-excitation of the hydrogen two-photon continuum (see, for example, Pottasch 1984; Osterbrock 1989). In Figure 4 the stellar continuum is that of a 45,000 K blackbody, and has been arbitrarily normalized so as to fit the continuum near 1300 Å, where it is the major contributor. It is clear that the central star has been detected, and that the nebular model gives a good description to the observed continuum in the 1200–8000 Å. The major apparent difference is the relatively small Balmer discontinuity seen in the optical spectra. However, a host of faint, unresolved emission lines, including the high members of the Balmer Series, combine to produce a quasi-continuum above the Balmer jump, as far as about Hδ. The true continuum placement is defined more nearly by the lower envelope of the flux measurements.

The accurate separation of the nebular and stellar components of the continuum allow us to determine a Zanstra temperature from a comparison of the flux emitted in the Hβ line, F(Hβ), with that of the stellar continuum in the V band (Å^{-1}), F_λ(V), according to the formula given by Pottasch (1984):

$$F(\mathrm{H}\beta)/F_\lambda(\mathrm{V}) = 3.95 \times 10^{-11} T_z^3 \, G_1(T_z) \times \{\exp\,[26650/T_z] - 1\}\,, \quad (4.1)$$

where the integral $G_1(T_z)$ is given by

$$G_1(T_z) = \int_{h\nu_1/\kappa T_z}^{\infty} x^2 (\exp\,[x] - 1)^{-1}\, dx\,. \quad (4.2)$$

The stellar flux from the continuum model showed in Figure 4 was measured in the range 5055 to 5945 Å and compared to the Hβ line flux from Meatheringham et al. (1988b). This gives a Zanstra temperature of T_z = 48,700 ± 1900 K, where the errors are due to the error in the determination of the absolute Hβ line flux (±0.07 dex) and in the placement of the stellar continuum in the continuum fit (±0.05 dex). The ionization

temperature and the Zanstra temperature are in excellent agreement, and it is therefore not necessary to invoke a "Zanstra discrepancy" in this case.

Finally, with this Zanstra temperature, we can estimate the stellar luminosity from the absolute luminosity of the central star in Figure 4, assuming that it radiates as a blackbody. From the measured flux at 1216 Å; 4.3×10^{-13} ergs cm^{-2} s^{-1} Å^{-1}, which should be almost entirely due to central star, we derive a luminosity of $7400 \pm 1200\ L_\odot$.

5. DISCUSSION

The model establishes the luminosity of the central star to be $7300 \pm 700\ L_\odot$. The luminosity of the PNN depends upon whether it is on a H-burning or He-burning track, which in turn depends on the phase of the thermal pulse cycle at which the transition to PN occurs. Dopita, Jacoby, & Vassiliadis (1992) argue that the distribution of the LMC PNN on the Hertzsprung-Russel Diagram strongly argues in favor of the hypothesis that the majority of these are helium-burners. For the hydrogen-burning objects, the core mass is well-determined, since the evolution to high temperature occurs at an almost constant luminosity, L, which may be expressed in terms of the core mass (Wood & Zarro 1981, Dopita et al. 1992):

$$(L/L_\odot) = 57340\{(M_c/M_\odot) - 0.507\}\ , \qquad (5.1)$$

from which we can derive the core mass given in Table 2, $M_c = 0.63 \pm 0.03\ M_\odot$. If helium-burning, the core mass is somewhat higher, about $0.67 \pm 0.03\ M_\odot$, according to the tracks of Vassiliadis (1992).

The combination of the UV and optical spectra has permitted us to derive accurate abundances, and to derive the carbon abundance for the first time. Although the heavier elements have abundances consistent with those expected in the LMC (Russell & Dopita 1990), the carbon abundance is well above that normally found in the LMC, and even exceeds the solar value. The C/O ratio of 2.2 is a clear indication that large amounts of dredge-up have occurred, and that this star is derived from a carbon star precursor. Values as high as this were also derived by Aller et al. (1987) for LMC PNs using spectra from *IUE*. For WS2 (SMP6), they find C/O = 2.7, and in WS 33 (SMP 78) the C/O ratio was estimated at 1.55.

The structure that we have derived from the nebula casts light on the early evolution of planetary nebula. The ratio of densities between the cloud and the intercloud components, ~ 50, is consistent with what would be expected for dense clouds of gas being ionized by an external source of UV photons, and having strong D-type ionization fronts at the boundary between the ionized and the unionized gas (Dyson 1968; Kahn 1969). Such a model would predict an expansion velocity for the ionized gas of about the isothermal sound speed, ~ 12 km s^{-1}, consistent with the observed expansion velocity; 11.3 km s^{-1}. Thus the expansion timescale we derive is in fact a measure of the time since the nebula began to be ionized, which we will call the ionization timescale.

This can also be estimated by consideration of the cloud component. Of the total output of ionizing photons from the central star $\sim 3.7 \times 10^{47}$ s^{-1}, $\sim 30\%$ are intercepted by the clouds. Because of the need to maintain the ionization in the dense gas around these clouds, few of these photons go into producing new ionization. If we take the ionization front to be strong-D, or D-critical, the speed of the ionization front is $\lesssim 10$ km s^{-1}, and the rate of outflow through the ionized layer will be ~ 5 km s^{-1}. At a hydrogen density of 1.6×10^6 cm^{-3}, this implies a mass flux of $\sim 1.7 \times 10^{-4}\ M_\odot$ yr^{-1} into the ionized gas. The same quantity can also be estimated more directly from the model, which shows that the layer of ionized gas is $\sim 4.1 \times 10^{13}$ cm thick. Assuming an average speed of flow through it of 5 km s^{-1}, it takes ~ 2.6 years for a parcel of gas to pass through the dense ionized region, which according to the model has a total mass of $4.1 \times 10^{-4}\ M_\odot$. The rate of production of ionized material is therefore $\sim 1.6 \times 10^{-4}\ M_\odot$ yr^{-1}. These two estimates are in good agreement. Given that the mass of the low-density ionized component in the model is $0.075\ M_\odot$, we can conclude that the nebula has an ionization age of about 500 years.

The difference between this and the estimate of ~ 2000 years (maximum) for the dynamical age can be ascribed to the fact that the rate of production of ionizing photons by the PNN is increasing rapidly. The ionization age given from consideration of the cloud component measures the timescale for the ionized mass to double at the current time, while the estimate based on the expansion timescale of the intercloud gas measures rather the timescale since ionization first began.

Models of the evolution of hydrogen burning PNN with LMC abundances by Vassiliadis (1992) show that, at the position of SMP 85 on the H-R diagram, about 800 years have passed since log $T_{\rm eff}$ became greater than 4.0, and that about 500 years have passed since log $T_{\rm eff}$ passed 4.5. For He-burning tracks the numbers are similar, 1000 and 600 years, respectively. These are in satisfactory agreement with the ionization timescale $500 < \tau_{\rm ion} < 2000$ years estimated above.

The expansion velocity of the atomic or molecular gas ejected just before the termination of the AGB phase of evolution must be rather low. This material, identified with the clouds, cannot have traveled more than the distance to the inner edge of the ionized nebula, 4×10^{16} cm since that time. Furthermore, it was ejected not less than 2000 years ago. This places an upper limit on the velocity of ejection of ~ 6 km s^{-1}.

We would like to estimate the mass-loss rate at the termination of the AGB evolution. However, this is neither trivial nor can it be reliably derived in a direct fashion from these observations. Let us apply, as a working hypothesis, the assumption that the outflowing wind has been broken up by a dynamical instability, either associated with the passage of the ionization front, or a result of Rayleigh-Taylor instabilities associated with the development of a fast stellar wind from the PNN. In this case, the clouds will have a characteristic size similar to that of the ionized flow region ($\sim 4 \times 10^{13}$ cm). To give a total covering factor of 0.3, we would then require $\sim 10^6$ of these in the ionized region. Since the sound crossing time of these clouds is much shorter than the evolution time, we can take the molecular gas to be in pressure equilibrium with the ionized flow. Assuming a temperature of ~ 100 K for the material, the density of the clouds would be $\sim 2 \times 10^8$ cm^{-3} and the cloud lifetime would then be of the same order as the ionization timescale of the nebula. The implies a reservoir of $0.06\ M_\odot$ of atomic gas to be added to the total amount of ionized gas, $0.075\ M_\odot$ out to 1.5×10^{17} cm. At an outflow velocity of 5 km s^{-1}, this implies an AGB mass-loss rate of $\sim 1.4 \times 10^{-5}\ M_\odot$ yr^{-1}. However, this estimate remains uncertain to about an order of magnitude.

6. CONCLUSIONS

In this paper, thanks to images and UV spectrophotometry from the *HST*, we have been able to produce a self-consistent

model for a second Magellanic Cloud planetary nebula. This proves that SMP 85 is a dense, young, carbon-rich object containing a substantial inner reservoir of unionized gas, probably in the form of many small cloudlets. We have directly detected the central star through its UV continuum emission, and from both Zanstra techniques the nebular modeling derive a stellar temperature of close to 46,000 $\pm$ 2000 K, a stellar luminosity of 7300 $\pm$ 800 $L_{\odot}$, a core mass of 0.63–0.67 $M_{\odot}$, and an age of 500–1000 years since ionization of the nebula first started. The expansion velocity of the atomic or molecular gas ejected just before the termination of the AGB phase of evolution must have been rather low, of order ~ 6 km s^{-1}.

The results described in this paper are based on observations with the NASA/ESA *Hubble Space Telescope*, obtained at the Space Telescope Science Institute, which is operated by the Association of Universities for Research in Astronomy, Inc., under NASA contract NAS5-26555. We thank D. J. Lindler who set up the procedure for reprocessing the data and provided the deconvolved images. M. A. D. acknowledges a grant from the International Science and Technology Department of Australian Department of Industry Technology and Commerce without which the modeling described would not have been possible.

REFERENCES

Aller, L. H., Keyes, C. D., Maran, S. P., Gull, T. R., Michalitsianos, A. G., & Stecher, T. P. 1987, ApJ, 320, 159
Balick, B. 1989, in IAU Symp. 131, Planetary Nebulae, ed. S. Torres-Peimbert (Dordrecht: Kluwer), 83
Barlow, M. J. 1989, in IAU Symp. 131, Planetary Nebulae, ed. S. Torres-Peimbert (Dordrecht: Kluwer), 319
Bessell, M. S. 1991, A&A, 243, L17
Binette, L., Dopita, M. A., & Tuohy, I. R. 1985, ApJ, 297, 476
Clegg, R. E. S., Harrington, J. B., Barlow, M. J., & Walsh, J. R. 1987, ApJ, 314, 551
Dopita, M. A., Ford, H. C., Bohlin, R., Evans, I. R., & Meatheringham, S. J. 1993, ApJ, 418, 804
Dopita, M. A., Ford, H. C., Lawrence, C. J., & Webster, B. L. 1985b, ApJ, 296, 390
Dopita, M. A., Ford, H. C., & Webster, B. L. 1985a, ApJ, 297, 593
Dopita, M. A., Jacoby, G. H., & Vassiliadis, E. 1992, ApJ, 389, 27
Dopita, M. A., & Meatheringham, S. J. 1991a, ApJ, 367, 115
———. 1991b, ApJ, 377, 480
Dopita, M. A., Meatheringham, S. J., Webster, B. L., & Ford, H. C. 1988, ApJ, 327, 639
Dyson, J. E. 1968, Ap&SS, 1, 388
Feast, M. W. 1988, in The Extragalactic Distance Scale, ASP Conf. Ser. No. 4, ed. S. van den Bergh & C. J. Pritchet (Provo: Brigham Young Univ. Press), 9
Feast, M. W., & Walker, A. R. 1987, ARA&A, 25, 345
Fitzpatrick, E. L. 1985, ApJ, 299, 219
Jacoby, G. H., Walker, A. R., & Ciardullo, R. 1990, ApJ, 365, 471
Kahn, F. D. 1969, Physica, 41, 172
Kaler, J. B. 1976, ApJS, 31, 517
Krist, J. 1992, The Tiny Tim User's Manual: Version 2.1 (Baltimore: STScI)
Lucy, L. B. 1974, AJ, 79, 745
Meatheringham, S. J., & Dopita, M. A. 1991a, ApJS, 75, 407
———. 1991b, ApJS, 76, 1085
Meatheringham, S. J., Dopita, M. A., Ford, H. C., & Webster, B. L. 1988a, ApJ, 327, 651
Meatheringham, S. J., Dopita, M. A., & Morgan, D. H. 1988b, ApJ, 329, 166
Osterbrock, D. E. 1989, Astrophysics of Gaseous Nebulae and Active Galaxies (Mill Valley: University Science Books)
Pottash, S. R. 1984, Planetary Nebulae (Dordrecht: Reidel)
Preite-Martinez, A., & Pottasch, S. R. 1984, in IAU Symp. 103, Planetary Nebulae, ed. D. R. Flower (Dordrecht: Reidel), 547
Russell, S. C., & Dopita, M. A. 1990, ApJS, 74, 93
———. 1992, ApJ, 383, 508
Sanduleak, N., MacConnell, D. J., & Philip, A. G. D. 1978, PASP, 90, 621 (SMP)
Seaton, M. J. 1979, MNRAS, 187, 73P
Stoy, R. W. 1933, MNRAS, 93, 588
Sutherland, R. S., & Dopita, M. A. 1993, ApJS, 88, 253
Vassiliadis, E. 1992, Ph.D. thesis, Australian National Univ., Canberra
Vassiliadis, E., Dopita, M. A., Morgan, D. H., & Bell, J. F. 1992, ApJS, 83, 87
Westerlund, B. E., & Smith, L. F. 1964, MNRAS, 127, 449
Wood, P. R., Bessell, M. S., & Dopita, M. A. 1986, ApJ, 311, 632
Wood, P. R., Meatheringham, S. J., Dopita, M. A., & Morgan, D. H. 1987, ApJ, 320, 178
Wood, P. R., & Zarro, D. M. 1981, ApJ, 247, 247